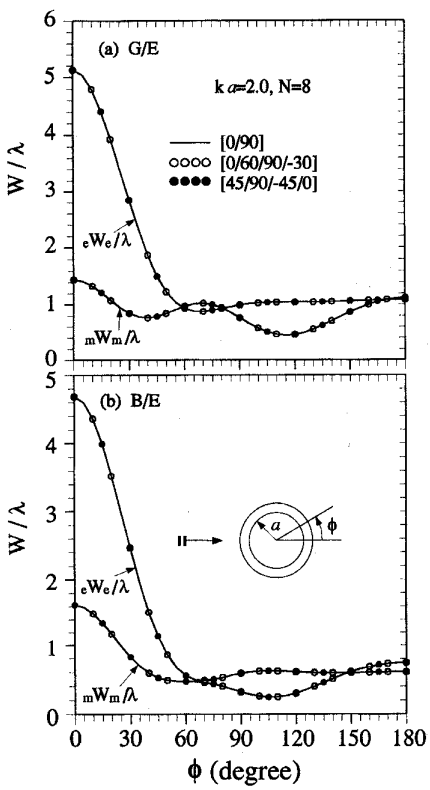

Fig. 11. Bistatic echo widths of composite cylindrical shells with three fiber orientation patterns which are [0/90], [0/60/90/−30], and [45/90/−45/0]. (TM and TE waves, $\theta = 90°$, $ka = 2$, $d = 0.127$ mm, $N = 8$.) (a) G/E and (b) B/E.

[8] M. Barabas, "Scattering of a plane wave by a radially stratified tilted cylinder," *J. Opt. Soc. Am.* vol. 4, no. 12, pp. 2240–2248, Dec. 1987.
[9] R. D. Graglia and P. L. E. Uslenghi, "Anisotropic layered absorbers on cylindrical structures," *Electromagnetics,* vol. 7, pp. 117–127, 1987.
[10] H. Massoudi and N. J. Damaskos, "Scattering by a composite and anisotropic circular structure: Exact solution," *Electromagnetics,* vol. 8, pp. 71–83, 1988.
[11] C.-C. Su, "Electromagnetic scattering by a dielectric body with arbitrary inhomogeneity and anisotropy," *IEEE Trans. Antennas Propagat.,* vol. 37, no. 3, pp. 384–389, Mar. 1989.
[12] C. M. Rappaport and B. J. McCartin, "FDFD analysis of electromagnetic scattering in anisotropic media using unconstrained triangular meshes," *IEEE Trans. Antennas Propagat.,* vol. 39, no. 3, pp. 345–349, Mar. 1991.
[13] X. B. Wu and W. Ren, "Scattering of a Gaussian beam by an anisotropic material coated conducting circular cylinder," *Radio Sci.,* vol. 30, no. 2, pp. 403–411, Mar. 1995.
[14] X. B. Wu, "Electromagnetic scattering from anisotropically coated impedance cylinder," *IEE Proc. Microwave Antennas Propag.,* vol. 142, no. 2, pp. 163–167, Apr. 1995.
[15] H. C. Chu *et al.,* "Diffraction from periodic composite structures," in *1995 URSI Int. Symp. EM Theory,* St. Petersburg, Russia, 1995, pp. 83–85.
[16] W. J. Gajda, "A fundamental study of the electromagnetic properties of advanced composite materials," Tech. Rep. RADC-TR-78-158, 1978.
[17] J. L. Allen *et al.,* "Electromagnetic properties and effects of advanced composite materials: Measurement and modeling," Tech. Rep. RADC-TR-78-156, 1978.
[18] J. H. Richmond, "Scattering by a dielectric cylinder of arbitrary cross-section shape," *IEEE Trans. Antennas. Propagat.,* vol. 13, no. 3, pp. 334–341, May 1965.
[19] ——— "TE-wave scattering by a dielectric cylinder of arbitrary cross-section shape," *IEEE Trans. Antennas. Propagat.,* vol. 14, no. 4, pp. 460–464, July 1966.
[20] C. Altman and K. Suchy, *Reciprocity, Spatial Mapping and Time Reversal in Electromagnetics.* Dordrecht/Boston/London: Kluwer, 1991, ch. 2.
[21] D. S. Jones, *Methods in Electromagnetic Wave Propagation.* Oxford, U.K., Oxford University Press, 1979, ch. 9.

Analysis of a Two-Port Flanged Coaxial Holder for Shielding Effectiveness and Dielectric Measurements of Thin Films and Thin Materials

James Baker-Jarvis and Michael D. Janezic

***Abstract*—A two-port flanged coaxial probe for measuring the dielectric and magnetic properties of thin material sheets is analyzed. Closed form solutions for the two-port scattering parameters are presented. The solution assumes an incident TEM wave together with evanescent TM_{0n} modes. Numerical results are obtained for both the forward and inverse problem. Computations indicate that at low frequencies the incident waves are almost totally reflected. As the frequency is increased, transmission through the sample increases. Experimental results compare closely with theory. The inverse solution yielded good permittivity determination for the cases tested. The technique should prove useful for nondestructive testing of circuit boards or substrates.**

***Index Terms*—Coaxial line, dielectric constant, flanged coaxial holder, loss factor, microwave measurements, nondestructive, open-ended probe, permeability measurement, permittivity measurement, shielding effectiveness, two port.**

I. Introduction

The goals of this paper are to present an exact solution of the boundary value problem that models a two-port flanged coaxial system, present results of the inverse solution, and compare the model's predictions to experimental results.

Processing control applications requires a relatively accurate, simple, nondestructive test of permittivity or permeability. The two-port flanged coaxial holder, as depicted in Fig. 1, fulfills these requirements. In addition, the flanged coaxial sample holder has been used for years as the American Society for Testing and Materials Standards (ASTM) measurement method for shielding effectiveness studies [1].

The flanged two-port coaxial holder allows a quick measurement of the insertion loss of a thin material as a function of frequency. For this reason, the technique has been used for electromagnetic interference studies [1]–[5]. In electromagnetic interference studies performed by Week [2], a two-port coaxial holder was used that had a continuous inner conductor across the flanges. A variation of this technique was adopted as the ASTM measurement method for shielding effectiveness [1], [4]. Later, a two-port flanged coaxial holder, where the center conductors terminated at the flange faces, was adopted as an ASTM standard measurement [5]. Numerical modeling of the two-

Manuscript received October 14, 1994; revised September 11, 1995.
The authors are with the Electromagnetic Fields Division, National Institute of Standards and Technology, Boulder, CO 80303 USA.
Publisher Item Identifier S 0018-9375(96)01881-9.

port coaxial holder device has also been performed [6]–[8]. Influences of the test fixture on measurement has been discussed in [9].

Potential applications include monitoring of circuit boards, substrates, and absorbing materials. The problem is to deconvolve the permittivity and, if need be, the permeability from measured scattering data. Previous studies have not attempted to perform the inverse solution for the permittivity and permeability from measured scattering data. This is due, at least in part, to the lack of an exact solution to the scattering problem.

II. Theory

The material under test is assumed to have a permittivity of $\epsilon_2^* = [\epsilon_{r2}' - j\epsilon_{r2}'']\epsilon_o = \epsilon_{r2}^*\epsilon_o$ and a permeability $\mu_2^* = [\mu_{r2}' - j\mu_{r2}'']\mu_o = \mu_{r2}^*\mu_o$, where ϵ_o and μ_o are the permittivity and permeability of vacuum. The coaxial line with inner dimension $2a$ and outer dimension $2b$ is filled with a material of permittivity $\epsilon_c^* = \epsilon_{rc}^*\epsilon_0$ and permeability $\mu_c^* = \mu_{rc}^*\mu_0$.

We will assume that the coaxial line operates at a frequency such that only the fundamental TEM mode is propagating. Evanescent TM_{0n} modes are also assumed to exist in the coaxial line near the probe ends. Including TM_{0n} modes in the coaxial line is necessary to match boundary conditions at the holder-material interface. TEM modes can exist in region 2; however, they should not be excited due to the symmetry of the excitation. The ground flanges and samples are assumed to extend to infinity in the radial direction. In applications, the diameter of the flanges and sample are made sufficiently large ($\geq$4b) to approximate this boundary condition.

The azimuthally symmetric H_ϕ mode in the coaxial line induces a H_ϕ magnetic field in the homogeneous and isotropic material under test. The magnetic field satisfies Helmholtz's equation

$$\left[\frac{\partial^2}{\partial\rho^2} + \frac{1}{\rho}\frac{\partial}{\partial\rho} - \frac{1}{\rho^2} + \frac{\partial^2}{\partial z^2} + k_i^2\right] H_{\phi i}(\rho, z) = 0 \tag{1}$$

in the coaxial line and sample region. The propagation constant in region (i) is $k_i^2 = \epsilon_{ri}\mu_{ri}\omega^2/c_V^2$, and c_V is the speed of light in vacuum.

The boundary conditions on the fields are

$$E_{\rho 1}(\rho, 0) = 0, \quad \rho \in [b, \infty], \quad \rho \in [0, a], \tag{2}$$

$$E_{\rho 3}(\rho, d) = 0, \quad \rho \in [b, \infty], \quad \rho \in [0, a], \tag{3}$$

$$E_{\rho 2}(\rho, 0_+) = E_{\rho 1}(\rho, 0_-), \tag{4}$$

$$E_{\rho 3}(\rho, d_+) = E_{\rho 2}(\rho, d_-), \tag{5}$$

$$H_{\phi 2}(\rho \to \infty, z) \to 0, \quad z \in [0, d], \tag{6}$$

$$H_{\phi 2}(\rho, 0_+) = H_{\phi 1}(\rho, 0_-), \tag{7}$$

$$H_{\phi 3}(\rho, d_+) = H_{\phi 2}(\rho, d_-), \tag{8}$$

$$E_z(a, z) = E_z(b, z) = 0, \quad z \in [-\infty, 0] \quad \text{and} \quad [d, \infty]. \tag{9}$$

For an incident wave traveling in the lower coaxial line, the radial component of the normalized solution in the coaxial line is a linear combination of TEM and TM_{0n} modes

$$E_{\rho 1}(\rho, z) = R_0(\rho)\exp(-\gamma_0 z) + \sum_{m=0}^{\infty} S_{11(m)} R_m(\rho) \cdot \exp[\gamma_{m(c)} z], \quad \rho \in [a, b]. \tag{10}$$

In the sample the spectrum is continuous and the electric field can be expressed as

$$E_{\rho 2}(\rho, z) = \int_0^\infty \zeta J_1(\zeta\rho)\frac{\gamma_2}{j\omega\epsilon_2^*}\{A(\zeta)\exp[-\gamma_2(z-d)] - B(\zeta)\exp[\gamma_2(z-d)]\}\, d\zeta, \quad \rho \in [0, \infty]. \tag{11}$$

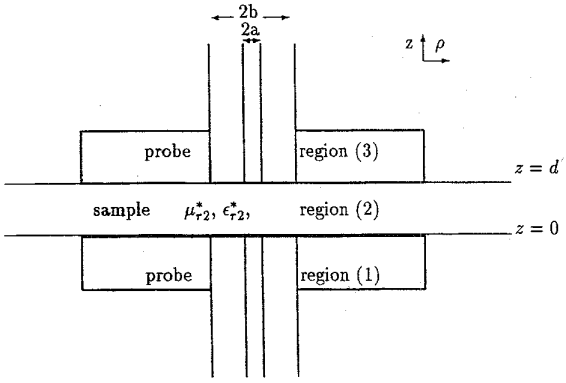

Fig. 1. The flanged coaxial holder with sample.

In the terminating coaxial line

$$E_{\rho 3}(\rho, z) = \sum_m S_{21(m)} R_m(\rho)\exp[-\gamma_{m(c)}(z-d)], \quad \rho \in [a, b] \tag{12}$$

$E_{\rho 1} = E_{\rho 3} = 0$ for $\rho > b$. The coaxial line TM_{0n} propagation constants are $\gamma_{n(c)} = \sqrt{k_{n(c)}^2 - (\omega/c_V)^2\epsilon_{rc}^*\mu_{rc}^*}$, where $k_{n(c)}$ are cutoff wavenumbers and (c) denotes coaxial line. Note that all of the TM_{0n} modes are evanescent. Also, $\gamma_2 = j\sqrt{k_2^2 - \zeta^2}$, if $\Re(k_2) > \zeta$, and $\gamma_2 = \sqrt{\zeta^2 - k_2^2}$ if $\Re(k_2) < \zeta$. Also, R_m are radial eigenfunctions. The magnetic fields can be calculated in a straight forward manner from the electric fields (10)–(12) by the impedance relation for TM_{0n} modes, $E_{\rho i}/H_{\phi i} = \pm\gamma_i/j\omega\epsilon_i^*$. The (+) sign is for forward traveling waves and (−) sign for reverse traveling waves. The solution of this boundary value problem can easily be shown to be unique.

III. Scattering Parameters

The scattering parameters may be constructed if we match at interfaces the Hankel transforms of (10)–(12) and analogous equations for the magnetic field, solve for coefficients, and then take inverse transforms. In particular, two independent vector relations can be obtained

$$\mathbf{Q}_1\vec{S}_{11} + \mathbf{Q}_2\vec{S}_{21} = \vec{P}_1 \tag{13}$$

and

$$\mathbf{Q}_2\vec{S}_{11} + \mathbf{Q}_1\vec{S}_{21} = \vec{P}_2. \tag{14}$$

Here $\vec{S}_{11}$ and $\vec{S}_{21}$ are the reflection and transmission vectors. The components of the matrices are

$$Q_{1mn} = \delta_{mn} + \frac{\epsilon_2^*\gamma_{n(c)}}{\epsilon_c^*}\int_0^\infty \cdot \frac{\zeta D_n D_m[\exp(2\gamma_2 d) + 1]}{\gamma_2[\exp(2\gamma_2 d) - 1]}\, d\zeta, \tag{15}$$

$$Q_{2mn} = -2\frac{\epsilon_2^*\gamma_{n(c)}}{\epsilon_c^*}\int_0^\infty \frac{\zeta D_n D_m \exp(\gamma_2 d)}{\gamma_2[\exp(2\gamma_2 d) - 1]}\, d\zeta, \tag{16}$$

$$P_{1n} = \delta_{n0} - \frac{\epsilon_2^*\gamma_{n(c)}}{\epsilon_c^*}\int_0^\infty \cdot \frac{\zeta D_n D_0[\exp(2\gamma_2 d) + 1]}{\gamma_2[\exp(2\gamma_2 d) - 1]}\, d\zeta, \tag{17}$$

and

$$P_{2n} = \frac{\epsilon_2^*\gamma_{n(c)}}{\epsilon_c^*}\int_0^\infty \frac{2D_0 D_n \zeta \exp(\gamma_2 d)}{\gamma_2[\exp(2\gamma_2 d) - 1]}\, d\zeta, \tag{18}$$

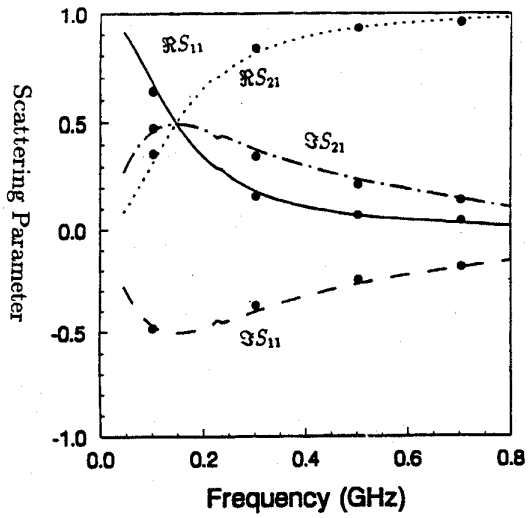

Fig. 2. The components of $S_{11(0)}$ and $S_{21(0)}$ as functions of frequency for polytetrafluoroethylene with $d = 1.8$ mm. The • denotes measured value and the line curves denote theoretical predictions. In this simulation $b = 38.404$ mm, $b/a = 2.3$, $\epsilon_{r2}^* = (2.04, -0.001)$, $\mu_{r2}^* = (1, 0)$ and six TM_{0n} modes were used.

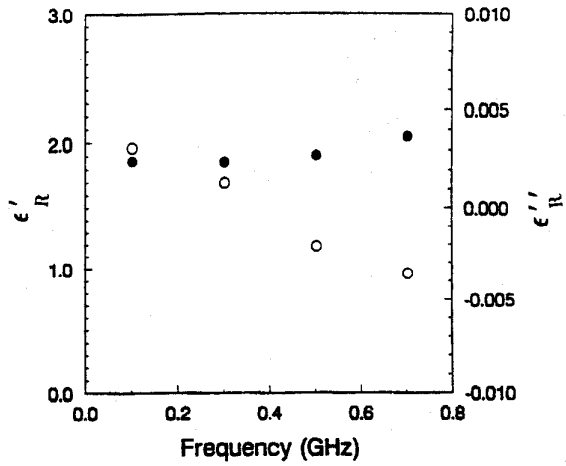

Fig. 3. Numerical determination of the permittivity as a function of frequency for a polytetrafluoroethylene sheet. The • symbols denote real permittivity and o symbols denote imaginary part of the permittivity. Six TM_{0n} modes were used. The combined standard uncertainty in ϵ'_{r2} is $u_c = 0.245$ and in ϵ''_{r2} is $u_c = 0.015$.

for $m, n = 0, 1, 2, 3, \cdots, N$. The coefficients

$$D_n(\zeta) = \int_a^b \rho J_1(\zeta\rho) R_n(\rho)\, d\rho \tag{19}$$

can be found analytically. For $n = 0$

$$D_0(\zeta) = \frac{1}{\sqrt{\ln\frac{b}{a}}} \int_a^b J_1(\zeta\rho)\, d\rho = \frac{1}{\sqrt{\ln\frac{b}{a}}} \frac{1}{\zeta} [J_0(\zeta a) - J_0(\zeta b)], \tag{20}$$

and otherwise

$$D_n(\zeta) = \int_a^b \rho R_n(\rho) J_1(\zeta\rho)\, d\rho = \frac{2}{\pi} \frac{C_n}{k_{n(c)}} \frac{1}{J_0[k_{n(c)}b]} \frac{\zeta}{k_{n(c)}^2 - \zeta^2} \cdot \{J_0(\zeta b) J_0[k_{n(c)}a] - J_0(\zeta a) J_0[k_{n(c)}b]\}. \tag{21}$$

Straightforward matrix manipulation of (13) and (14), assuming no singular matrice inverses are encountered, yields the following solution for the forward problem:

$$\vec{S}_{21} = [\mathbf{Q}_1 - \mathbf{Q}_2\mathbf{Q}_1^{-1}\mathbf{Q}_2]^{-1}(\vec{P}_2 - \mathbf{Q}_2\mathbf{Q}_1^{-1}\vec{P}_1) \tag{22}$$

and

$$\vec{S}_{11} = \mathbf{Q}_1^{-1}(\vec{P}_1 - \mathbf{Q}_2\vec{S}_{21}). \tag{23}$$

The first components in $\vec{S}_{11}$ and $\vec{S}_{21}$ are the measured TEM mode reflection coefficients obtained by a network analyzer.

IV. Numerical and Experimental Results

Measurements were made by placing a thin material between the flanges of two-port 14 mm and 77 mm coaxial holders. The system was calibrated so the reference planes were at the flange faces. The scattering parameters were then measured from 50 MHz to 2 GHz. It is important to have good contact between the sample and the coaxial flanges. Contact can be enhanced by use of silver pastes [5]. Plastic bolts were used between the flanges [5]. Influences of the test fixture on measurement has been summarized in [9]. In particular, care must be taken in the measurement of conductor-loaded plastics [9].

In order to check the solution, numerical solutions of (22) and (23) were generated. In Fig. 2, for given permittivity and permeability, the reflection coefficient of polytetrafluoroethylene as a function of frequency is plotted and compared to experimental data. We see a decrease in transmission and increase in reflection as frequency decreases. In Fig. 3 the calculated permittivity is displayed. The numerical solution was accomplished by solving (22) and (23) using a Newton–Raphson technique for the permittivity. As indicated in Fig. 3, we obtained good results for the calculated permittivity.

V. Conclusions

We have presented an exact analytical solution to a model of an idealized two-port flanged coaxial fixture. The solution can be expressed compactly using matrix algebra. The numerical work indicates that material parameters can be obtained by solving the inverse problem. At low frequency, evanescent fields protrude a short distance from the coaxial line ends into the sample. At these frequencies the system acts essentially as two independent open-ended coaxial probes; therefore, the reflection coefficient is high. As the frequency increases, some of the field energy transfers through the material to the other coaxial line. Consistent with this interpretation, data plotted in Fig. 2 verify that transmission increases as frequency increases; reflection also increases as frequency decreases.

The model is valid for frequencies where the field is confined to a region around the coaxial line ends and does not enter the flange regions appreciably. For lower permittivity materials this constraint is not hard to satisfy. Subject to these limitations on the frequency and sample thickness, the technique appears to be a viable method for extracting the dielectric and magnetic material properties of thin materials. The materials may be conductive or dielectric insulators.

Acknowledgment

The authors would like to thank C. Jones and J. Grosvenor for help with the experiments, and E. Vanzura and A. Ondrejka for their discussions.

REFERENCES

[1] "ASTM-E57 and ASTM-D4935 standard for measuring the shielding effectiveness in the far field," *1995 Annu. Book of ASTM Standards,* vol. 10.02, 1995.

[2] R. A. Week, "Thin film shielding for microcircuit applications and a useful laboratory tool for plane-wave shielding evaluations," *IEEE Trans. Electromag. Compat.,* vol. EMC-10, pp. 105–112, Mar. 1985.

[3] P. F. Wilson and M. T. Ma, "Factors affecting material shielding effectiveness measurements," in *IEEE Nat. Symp. Electromag. Compat. Proc.,* Aug. 1985, pp. 29–33.

[4] A. R. Ondrejka and J. W. Adams, "Shielding effectiveness (SE) measurement techniques," in *IEEE Nat. Symp. Electromag. Compat. Proc.,* Apr. 1984, pp. 249–256.

[5] J. W. Adams and E. Vanzura, "Shielding effectiveness measurements of plastics," Nat. Bureau Standards (U. S.) Interagency Rep. IR-85-3035, Nat. Bureau Standards, 1986.

[6] J. Waymond and R. Scott, "Accurate modeling of axisymmetric two-port junctions in coaxial lines using the finite element method," *IEEE Trans. Microwave Theory Tech.,* vol. 40, pp. 1712–1715, Aug. 1992.

[7] E. Marouby, M. Aubourg, and P. Guillon, "Application of the finite element method to the design of transitions between coaxial lines," *Proc. Inst. Elec. Eng.,* vol. 137, pt. H, Aug. 1990.

[8] G. M. Wilkins, J. Lee, and R. Mittra, "Numerical modeling of axisymmetric coaxial waveguide discontinuities," *IEEE Trans. Microwave Theory Tech.,* vol. 39, p. 88, Aug. 1991.

[9] J. Catrysse, M. Delesie, and W. Steenbakkers, "The influence of the test fixture on shielding effectiveness measurements," *IEEE Trans. Electromag. Compat.,* vol. 34, pp. 348–351, Aug. 1992.

Scattering from an Infinite Conducting Cylinder Covered with a Finite Two-Layer Dielectric Coating (Modal Approach)

Kaveh Heidary

Abstract— **The electromagnetic scattering problem of a conducting infinite circular cylinder partially shielded with a finite two-layer dielectric coating has been analyzed. Cylindrical eigenfunctions with unknown modal coefficients are used to expand the interior EM fields in terms of Fourier–Bessel series. Enforcing field boundary conditions at the dielectric-dielectric interface leads to a single set of modal coefficients for field expansions inside the inner and the outer dielectric layers. Replacing the dielectric coating with the induced polarization sources and utilizing pertinent Green's functions, the dielectric-scattered fields are then formulated in terms of the modal coefficients. Imposing field equivalence conditions yields sets of linear algebraic equations for numerical computation of the unknown modal coefficients and subsequently other parameters of interest. Computed backscattered fields based on the modal technique developed here are compared to experimental and numerical data obtained for the 2-D problem of a dielectric coated conducting cylinder.**

I. INTRODUCTION

Cylindrical structures, due to their widespread utility and mathematical simplicity, have been the subject of numerous studies over the course of many decades. A class of 2-D cylinders with surfaces coincident with the coordinate surfaces of an orthogonal system in which the Helmholtz equation is separable are amenable to exact formulation by utilizing cylindrical eigenfunction expansions [1]–[6].

Manuscript received August 22, 1994; revised September 7, 1995.
The author is with Matrix Technologies, Pittsburgh, PA 15228 USA.
Publisher Item Identifier S 0018-9375(96)01887-X.

The integral equation technique has been applied to treat the 2-D cylinder problem with arbitrary cross-section shape [7]–[11]. Both volume and surface equivalence methods have been employed in the integral equation formulations of the dielectric cylinder problem. Impediments associated with the spurious near-resonant solutions encountered in the surface integral formulation are rectified by applying the extended boundary condition method [12], [13]. High-frequency asymptotic techniques have been applied to treat the infinite conducting cylinder problem [14], [15]. Scattering from semi-infinite and finite conducting circular cylinders have been tackled, respectively, by the Weiner–Hopf solution and the spectral theory of diffraction [16]–[18]. Semi-empirical methods in conjunction with geometrical optics have been proposed and yielded reasonable results for the dielectric coated infinite cylinder problem [19]. The finite dielectric cylinder problem has been analyzed by applying moment method formalism to the volume integral equation [20].

Radar antenna blockage by an infinite conducting cylinder has been studied by utilizing cylindrical wave functions and superposition over the radiating aperture [21], [22]. A cylindrical obstruction situated near the main beam of a radar antenna can result in a substantial degradation of the radar performance. Performance of shipboard antennas, for example, may be impaired due to blockage of the antenna beam by the ship mast and yardarm. A dielectric coating attached to the conducting cylinder can result in abating the scattered field along particular directions and somewhat alleviating the blockage problem. Experimental results pertaining to the effect of an absorptive coating on the blockage reduction are reported in [22]. A thorough analysis of the 2-D problem of a dielectric coated conducting cylinder was carried out by Tang [6]. Numerical and experimental data in [6] illustrate the strong influence of the dielectric coating on the backscattered field. A finite dielectric coating cladding an infinite conducting cylinder and covering the 3 dB beamwidth of the antenna vertical pattern is virtually indistinguishable from an infinite dielectric coating in the horizontal plane. Detailed analysis of a partially shielded infinite conducting cylinder is presented by the author in an earlier paper [23]. It has been demonstrated that a significant reduction in the backscattered field, with respect to that of the bare conducting cylinder, can be achieved over relatively wide frequency ranges. Effects of coating height, thickness, and permittivity on the backscattered field were studied in [24].

This paper considers the 3-D scattering problem of a conducting infinite circular cylinder clad by a finite-length dielectric sheathing composed of two homogeneous layers. The formulation presented here can be applied to a multiple-layer coating without major modifications. A multiple layer coating offers greater flexibility in selecting the thickness and permittivity of individual layers for optimal performance. In certain applications, for instance, it may be desired to keep the backscattered field below a threshold level throughout a range of frequencies. The superiority of multiple-layer coatings in such applications is manifested through a higher degree of freedom in parameter selection.

The method of analysis applied here parallels the modal technique of [23]. Electromagnetic fields inside each dielectric layer are expressed in terms of a TM (to the cylinder axis) and a TE potential. Whole-body expansion functions based on the cylindrical wave functions in respective dielectric layers are utilized in the interior potential function expansions. Modal potential functions with unknown modal coefficients yield Fourier–Bessel series expansions for the interior potential functions inside each dielectric layer. Impos-